JOURNAL OF SOLID STATE CHEMISTRY 108, 37–45 (1994)

Jahn–Teller Distortions and Cation Distribution in Cu(II)–*Me*(II) [*Me* = Mg, Co] Hydroxide Nitrate Solid Solutions—A Spectroscopic and Structural Study

M. Atanasov,* N. Zotov,* C. Friebel,† K. Petrov,* and D. Reinen†,[1]

*Bulgarian Academy of Sciences, Sofia, Bulgaria; †Fachbereich Chemie and Zentrum für Materialwissenschaften der Universität, D35032 Marburg, Germany

Received December 29, 1992; accepted April 15, 1993

Mixed crystals $Me_{2-x}Cu_x(OH)_3NO_3$ (*Me*: Co^{2+}, Mg^{2+}) were investigated by spectroscopic (EPR, ligand field), structural, and magnetic methods. For $0 < x < 1$ the $Me(OH)_4(ONO_2)_2$ site (1) is occupied with great preference by Cu^{2+}, because it provides a larger Jahn–Teller distortion than the $Me(OH)_5(ONO_2)$ site (2). The magnetic exchange coupling between the Cu^{2+} polyhedra is rather large and of antiferromagnetic nature. The electronic and elastic interactions underlying the observed cooperative Jahn–Teller order pattern are analyzed.

I. INTRODUCTION

Structure and bonding in layered transition metal hydroxide nitrates and their solid solutions have been studied extensively, since these compounds are efficient precursors for the synthesis of simple and complex metal oxides with interesting electric, magnetic, and catalytic properties (1). In particular, copper(II)–cobalt(II) hydroxide nitrate solid solutions, $Co_{2-x}Cu_x(OH)_3NO_3$, have been investigated by means of X-ray powder diffraction (2), IR spectroscopy (3), and thermal analysis (4). The structure of monoclinic $Cu_2(OH)_3NO_3$ (5) can be traced back to that of $Mg(OH)_2$ by the substitution of one-fourth of the OH^- by nitrate ligands in an ordered way. It consists of $^2_\infty[Cu(OH)_{1.5}(ONO_2)_{0.5}]$ layers of octahedra sharing common edges (Fig. 1). Adjacent layers are held together by hydrogen bonds. One of the oxygen atoms of each NO_3 group is bonded to three copper ions. Cu^{2+} occupies two nonequivalent positions. Cu(1) is coordinated by four equatorial OH groups at an average distance of 1.96_5 Å and two oxygen atoms belonging to NO_3 groups at ≈2.40 Å. Cu(2) is coordinated by four equatorial OH groups at 1.99_5 Å and by one OH^- and one NO_3^- group at 2.31 and 2.39 Å, respectively, in the axial directions. The coordination polyhedra of Cu(2) are less distorted than those of Cu(1) (2). The polyhedron connection pattern is shown in Fig. 1.

[1] To whom correspondence should be addressed.

Cu^{2+} (d^9) in octahedral coordination is Jahn–Teller unstable. Vibronic coupling of the electronic ^2E_g ground state wave functions to the normal ε_g mode lowers the symmetry and energy of the initial configuration (Fig. 2.). It has been shown experimentally that even when the ligands are different, as in the compounds studied here, vibronic coupling is still operative (pseudo-Jahn–Teller effect) (6, 7). Unfortunately, structural single crystal data for the compounds $Me_2(OH)_3NO_3$ with *Me* = Co^{2+}, Mg^{2+} are not available. It is expected, however, that the deviations of the polyhedra from regular octahedral symmetry are much less than in case of Cu^{2+}. Looking at the local distortions of the CuO_6 polyhedra in $Cu_2(OH)_3NO_3$ one would expect that in Cu(II)–*Me*(II) (*Me* = Mg, Co) hydroxide nitrate solid solutions, non-Jahn–Teller ions such as Mg^{2+} and Co^{2+} would substitute preferentially for the copper atoms in the less distorted site (2). Support of this prediction is provided by IR analysis (3) and the compositional deformation tensor (8) of Cu(II)–Co(II) hydroxide nitrates.

In the following we report the structural results and the optical spectra of mixed crystals $Me_{2-x}Cu_x(OH)_3NO_3$ (*Me* = Co, Mg) as well as EPR results for Cu^{2+} in $Mg_2(OH)_3NO_3$. Our aim is to analyze the substitution mechanism and the polyhedron distortions induced by Cu^{2+} in dependence on the copper concentration. We finally discuss how the structural peculiarities of the offered sites (presence of strain due to different ligands in the coordination sphere of Cu^{2+}) and the local and cooperative vibronic interations in and between the CuO_6 octahedra, respectively, influence the cation distribution.

In a subsequent report we will present results of the $Cu_xZn_{1-x}(OH)_3NO_3$ mixed crystal series with layered and chain-type structures.

II. EXPERIMENTAL

Hydroxide nitrate solid solutions $Me_{2-x}Cu_x(OH)_3NO_3$, where x = 0.0, 0.21, 0.37, 0.57, 0.78, 0.95, 1.14, 1.32,

0022-4596/94 $6.00

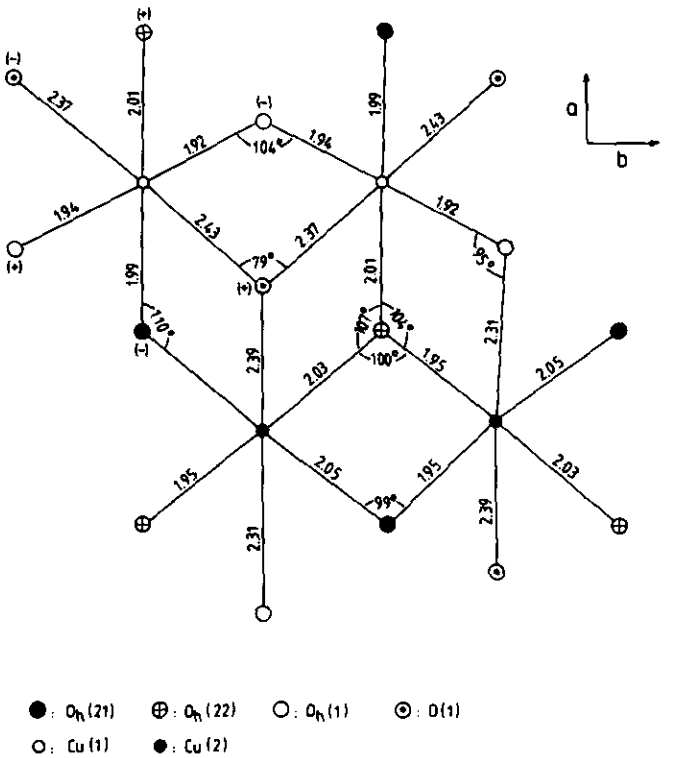

FIG. 1. Section from the layer structure of $Cu_2(OH)_3NO_3$. The two magnetically different Cu^{2+} ions lie approximately in the figure plane, (+) and (−) denoting positions above and below this plane. $O_h(21,22)$ and $O_h(1)$ refer to OH^- ligands, involved in short and also long Cu–O bonds, respectively; O(1) is the ligator atom of the NO_3^- group, bonded to Cu^{2+} (nomenclature following Effenberger (5)).

1.42, 1.75, and 2.00 for $Me = Mg^{2+}$ and $x = 0.0$, 0.20, 0.35, 0.49, 0.57, 0.69, 0.94, 1.20, 1.47, 1.73, and 2.00 for $Me = Co^{2+}$, have been prepared according to the following procedure.

Equal volumes of 0.5 *M* sodium hydroxide and copper(II) nitrate solutions were added simultaneously and at the same rate (double-jet technique) to a preset quantity of hot (100°C) solutions of 3.5 *M* cobalt(II) or magnesium(II) nitrate with continuous stirring. Constant suspension volume was maintained during the precipitation by controlling the rates of evaporation from and addition to the solutions. The amount of NaOH used corresponded to a 1.5 molar ratio with respect to the divalent metal cations. In order to obtain different Cu/*Me* atomic ratios in the precipitates, the concentration of the copper(II) nitrate solution used for different samples was varied between 0.0 and 0.5 *M* (9). The hydroxide nitrate phases were filtered from the mother solutions, washed with water and ethanol, and dried. The total content of the divalent metals in the samples was determined using routine complexometric methods. The amount of copper was determined iodometrically.

The X-ray diffraction measurements of the $Me_{2-x}Cu_x(OH)_3NO_3$ samples were carried out using a DRON-3 powder diffractometer (filtered CoK_α radiation, scintillation counter, continuous strip chart recorder). The unit cell parameters were refined from diffraction data collected at an angular speed of $\frac{1}{4}°$ min^{-1} in the 2θ range 10–75° using the least-squares computer program PDI (10).

The diffuse reflectance spectra of all prepared samples were recorded on a Perkin–Elmer 330 UV–vis–near IR spectrometer at room temperature and on a Zeiss PMQ II spectrophotometer (Infrasil) at 295 and 5 K. Freshly sintered MgO (8000–30,000 cm^{-1}) was used as a standard. The reflectance data were converted into absorption values $\log(k/s)$ following the theory of Schuster, Kubelka, and Munk (11).

EPR spectra at room temperature and ≈130 K were taken with both a Varian instrument (35 GHz, Q band) and a Bruker *X*-band spectrometer. DPPH ($g = 2.0037$) was used as an internal standard. Magnetic susceptibility measurements were performed in an external magnetic field of 10 and 30 kG in the temperature range between 1.8 and 300 K with a SQUID magnetometer (Quantum Design).

III. RESULTS AND DISCUSSION

1. *Optical Spectra of Mixed Crystals* $Me_{2-x}Cu_x(OH)_3NO_3$[*Me*: Co^{2+}, Mg^{2+}]

The diffuse reflectance spectra of $Co_{2-x}Cu_x(OH)_3NO_3$ compounds are presented in Fig. 3. In the case of $Co_2(OH)_3NO_3$ a broad band centered at ≈8000 cm^{-1}, a weak shoulder at about 16,000 cm^{-1} and a second band centered at ≈19,500 cm^{-1} are observed. The absorptions at 5200 and 7200 cm^{-1} are due to overtone excitations of the OH^- ligands. The origin of the peak at 22,800 cm^{-1} remains unclear. The main features of the spectrum of $Co_2(OH)_3NO_3$ are consistent with octahedral symmetry, the bands 8000, 16,000, and 19,500 cm^{-1} being assigned to the $a^4T_{1g}(F) \rightarrow a^4T_{2g}(F)$, $\rightarrow a^4A_{2g}$, and $\rightarrow b^4T_{1g}(P)$ transitions, respectively. One has to realize, however, that these bands are the result of an overlap of transitions due to two different sites, which are split by lower-symmetry perturbations in addition. With the proposed assignment a ligand field parameter of $\Delta \approx 8500$ cm^{-1} and a Racah parameter of $B \approx 840$ cm^{-1} are obtained. They are consistent with those calculated from the band positions of $Co(OH)_2$ (12): $\Delta \approx 8250$ cm^{-1} and $B \approx 810$ cm^{-1}.

The spectrum of $Cu_2(OH)_3NO_3$ at liquid helium temperature (Fig. 4) is a superposition of at least three broad bands centered at about 9000, 12,000, and 16,000 cm^{-1}. The spectra of the mixed crystals with low Cu^{2+} concentrations are substantially different. The EPR spectra indicate that one site is occupied in these cases ($x < 1$) nearly

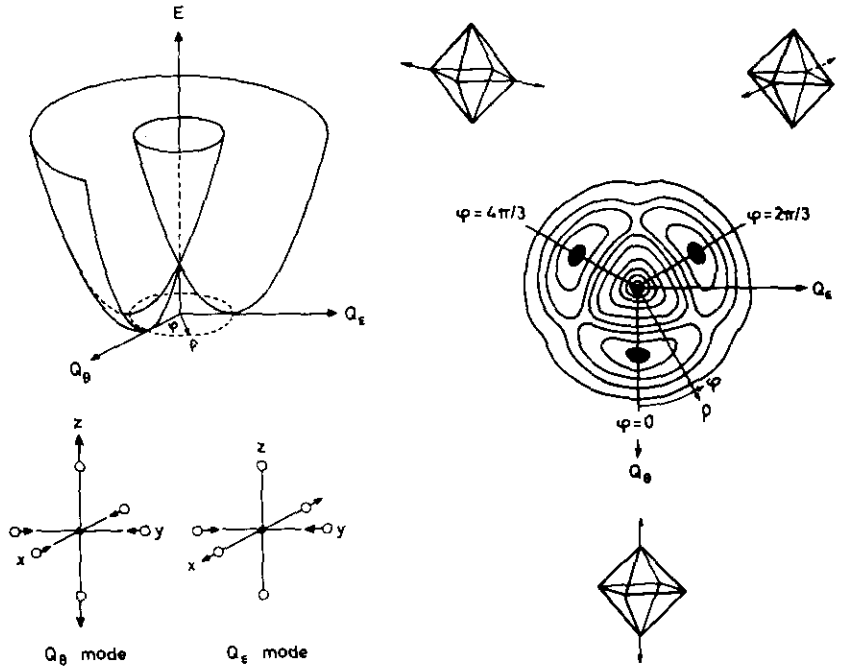

FIG. 2. Potential surface of the ^2E_g ground state as a result of linear $E \otimes \varepsilon$ vibronic coupling. The influence of higher order coupling terms is illustrated in a cross section perpendicular to the energy axis (ρ, φ: radial and angular distortion parameters, respectively). The minima at φ = 0, 120, and 240° correspond to octahedra, tetragonally elongated in one of the directions of the C_4 axes. The vibrational ε mode components are also shown.

exclusively (see below). The assignment of the observed *d–d* transitions is performed assuming tetragonally elongated octahedra with C_{4v} symmetry, yielding $^2B_1$, $^2A_1$ and $^2B_2$, ^2E split terms originating from the ^2E_g and $^2T_{2g}$ states in the O_h parent symmetry. We assign the two bands of predominant intensities at 16,000 and 13,000 cm^{-1} in the spectra with small x values to the transitions $^2B_1 \rightarrow {}^2E$ and $^2B_1 \rightarrow {}^2B_2$, $^2A_1$, respectively. A ground state splitting of 13,000 cm^{-1} is supported by two arguments. First, this splitting should be smaller than the one for $Ba_2Cu(OH)_6$ (Table 1), because the extent of polyhedron elongation is comparatively less distinct in our case. Second, the intensity distribution between the two bands strongly supports the proposed assignment. The comparison of the spectrum of $Cu_2(OH)_3NO_3$ with that of the mixed crystal with x = 0.21 (Fig. 4) clearly reveals that a second set of bands at lower energies is present. In a very rough consideration we may deduce two absorptions at about 9000 and 13,000 cm^{-1} with the tentative assignment given in Table 1. In any case and independent of the numerical interpretation it is clear that the spectrum at higher energies is due to the more distorted Cu(1) polyhedron. Apparently the site with the higher Jahn–Teller stabilization energy is preferentially occupied at low x values, and distinct changes of the spectra occur only at about $x > 1.0$. Size effects should not play any significant role, because Mg^{2+}, Co^{2+}, and Cu^{2+} have nearly equal ionic radii. It is further interesting that peaks of very small intensity at 8500 and 9200 cm^{-1}, obviously due to the less distorted Cu(2) polyhedron, appear already at small Cu^{2+} concentrations. The interpretation concerning the preference of Cu^{2+} for site (1) is also strongly supported by the ligand field spectra of mixed crystals $Co_{2-x}Cu_x(OH)_3NO_3$ (Fig. 3). It is nicely seen that an additional spectrum with a band at 16,000 cm^{-1} and a shoulder around 13,000 cm^{-1} appears with increasing intensity if x changes from 0 to about 1.0. These bands are clearly due to Cu(1) polyhedra. Only for $x > 1$ an absorption in the spectral region between 8000 and 13,000 cm^{-1} is observed, which is obviously caused by an occupation of site (2) by Cu^{+2} and which overlaps the spectrum characteristic for the more strongly distorted Cu(1) polyhedron.

2. *EPR Spectra of Mixed Crystals* $Mg_{2-x}Cu_x(OH)_3NO_3$

The EPR spectrum of the mixed crystal with x = 0.21 (Fig. 5) is indicative of only one species and characteristic for Cu^{2+} in a tetragonally elongated coordination [$^2B_1$ ($d_{x^2-y^2}$) ground state] with $g_\parallel = 2.315$ and $g\perp = 2.055$ (Q-band spectrum, Table 1). The hyperfine coupling of the unpaired electron with the nuclear spin of Cu^{2+} ($I = \frac{3}{2}$) is nicely seen. While the hyperfine splitting of $g_\parallel$ is ob-

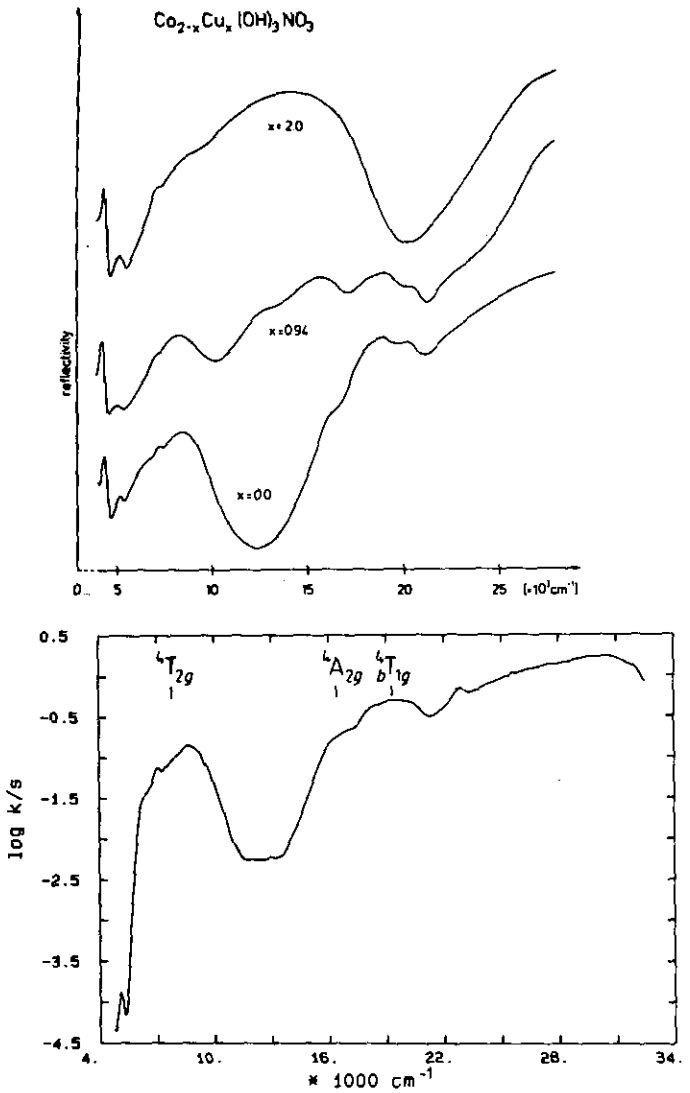

FIG. 3. Diffuse reflectance spectra of mixed crystals $Co_{2-x}Cu_x(OH)_3NO_3$ at room temperature (above, intensity in arbitrary units (reflectivity)). The spectrum of $Co_2(OH)_3NO_3$ at 5 K is shown below. The given assignment in O_h notation averages over the energy positions, due to two sites and symmetry splittings. Absorptions at 4500, 5200, and 7200 cm^{-1} are caused by OH overtone modes (see text).

served in X and Q band, $A\perp$ is only resolved at the lower frequency ($|A_\parallel| = 175 \cdot 10^{-4}\,cm^{-1}$, $|A\perp| = 28 \cdot 10^{-4}\,cm^{-1}$). A weak isotropic signal with $g_i = 2.14$, close to the mean g value $g_{av} = (\frac{1}{3})(2g\perp + g_\parallel)$, is also visible and presumably due to exchange coupling. This argument is supported by the observation, that the line width of this signal is smaller at X-band frequency by a factor of about five. With increasing Cu^{2+} concentration the $g_\parallel$ signal strongly broadens and the hyperfine structure finally disappears at $x > 0.57$. The $g\perp$ signal is continuously lowered in intensity but is still detected up to $x \approx 1.5$. No distinct temperature and concentration dependence of the g values is apparent.

From the g values, characteristic for a $(d_{x^2-y^2})$ ground state,

$$g_\parallel = g_0 + 8u_\parallel$$
$$g\perp = g_0 + 2u\perp \quad u_i = k_i^2 \cdot \lambda_0/\Delta_i \,(i = \parallel, \perp), \qquad [1]$$

orbital contributions $u_\parallel = 0.039$ and $u\perp = 0.027$ are derived. Assuming that the Cu (1) polyhedron induces the EPR spectrum ($\Delta_\parallel = E(^2B_1 \rightarrow {}^2B_2) \simeq 13{,}000\ cm^{-1}$; $\Delta\perp = E(^2B_1 \rightarrow {}^2E) \simeq 16{,}000\ cm^{-1}$) covalency factors $k_\parallel = 0.78$ and $k\perp = 0.72$ are estimated, in agreement with those reported for $Ba_2Cu(OH)_6$ (13) and other oxidic Cu^{2+} compounds (14) (Table 1).

The hyperfine tensor components make it possible to estimate the mixing coefficient of the $(d_{x^2-y^2})$ orbital in the ground state molecular orbital:

$$\psi_g = \alpha d_{x^2-y^2} - \alpha' L_{x^2-y^2}, \qquad [2]$$

where $L_{x^2-y^2}$ is the symmetry-adapted combination of ligand orbitals. The corresponding equations are

$$A_\parallel = P\{(-\kappa - 4/7)\,\alpha^2 + (3/7)\,(g\perp - g_0) + g_\parallel - g_0\}$$
$$A\perp = P\{(-\kappa + 2/7)\,\alpha^2 + (11/14)\,(g\perp - g_0)\}. \qquad [3]$$

The scaling factor $P = g_e g_N \beta_e \beta_N \langle r^{-3}\rangle$ has been estimated as $360 \times 10^{-4}\ cm^{-1}$ for Cu^{2+} (15, 16). κ is the Fermi contact term with a value of 0.43 (17). A mixing coefficient of $\alpha = 0.90_5$, indicating a rather ionic bond, correlates with $A_\parallel$ and $A\perp$ values of -174 and $-27 \times 10^{-4}\ cm^{-1}$, respectively. Negative $A_\parallel$ and negative or vanishing $A\perp$

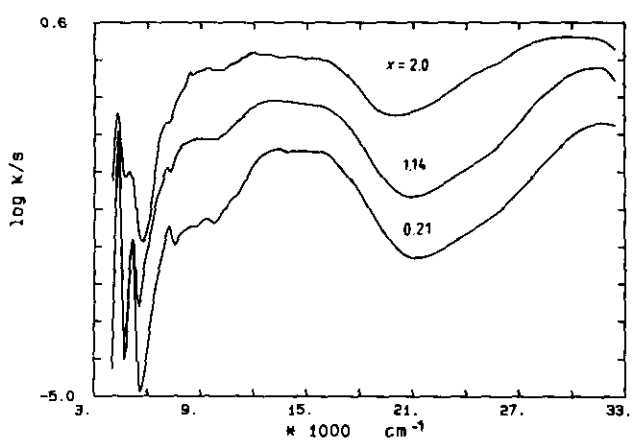

FIG. 4. Diffuse reflectance spectra of $Mg_{2-x}Cu_x(OH)_3NO_3$ (5 K). See also remark concerning OH overtone modes in caption Fig. 3.

TABLE 1
Optical Transition Energies (cm^{-1}), g values, and Geometric Parameters in Some Cu^{2+} Containing Compounds

			Cu^{2+} in $Mg_2(OH)_3NO$	
	$Ba_2Cu(OH)_6$[a]	Ba_2CuWO_6[a]	site 1	site 2
$^2B_1 \rightarrow {}^1A_1$	15,000	8,000	≈13,000	≈9,000[b]
$^2B_1 \rightarrow {}^2B_2$	14,000	9,200	≈13,000	≈9,000[b]
$^2B_1 \rightarrow {}^2E$	16,000	11,800	≈16,000	≈13,000
$g_\parallel$	2.29_1	2.44_2	2.31_5	—
$g_\perp$	2.05_2	2.07_2	2.05_5	—
R_e(Å)	1.96	2.00	≈1.96_5[c]	≈1.99_5[c]
R_a(Å)	2.80	2.38	≈2.40[c]	≈2.35[c]
ρ(Å)	0.51	0.97	0.51	0.41

[a] Data from Ref. (13).
[b] 8500 and 9200 cm^{-1} (see text and spectrum with $x = 0.21$ in Fig. 4).
[c] Structural results from Ref. (5).

values are indeed characteristic for elongated Cu^{2+} octahedra (17). The fluoride ligand induces coefficients α around 0.92 (17), while oxygen exhibits a wide range of values between 0.84 and 0.89 (18). OH^- has apparently an intermediate position, in agreement with nephelauxetic ratios $\beta = B/B_0$ for Ni^{2+} in oxides ($\simeq 0.82$) (19), in $Ni(OH)_2$ (0.89) (12), and in fluorides (0.92) (17).

In order to analyze the EPR results some basic understanding of the strength of the exchange interactions between the Cu^{2+} polyhedra, which are strongly interconnected via common edges, is necessary. The extent of this coupling can be estimated by the magnitude of the antiferromagnetic constant J^{af}. It has been shown that J^{af} can be expressed as a function of the bridging O–M–O angle α (20):

$$J^{af} = |J_0|\cos^2\alpha/(1 - \cos\alpha)^2 \qquad [4]$$

Based on this consideration and utilizing the geometrical sketch in Fig. 1 it follows that the bridging angles α are mostly significantly larger than 90° (typically 104°). The nonorthogonality of the magnetic orbitals for such a pathway in hydroxo dimers of Cu^{2+} leads to antiferromagnetic exchange constants $J \approx -100\ cm^{-1}$ (21), which value is large enough to suppress any EPR spectrum. Although the ability of the OH group to mediate supperexchange coupling in $Cu_2(OH)_3NO_3$ may be weakened because it is shared between three atoms, we believe that strong antiferromagnetic coupling is still present. This is supported by the magnetic data. The magnetic susceptibility of $Cu_2(OH)_3NO_3$ shows a maximum at $T_N = 7.4$ K, indicating a low-dimensional magnetic system. This maximum vanishes when doping with Mg^{2+}. The effective magnetic moment of $Cu_xMg_{2-x}(OH)_3NO_3$ mixed crystals per Cu^{2+} ion decreases with increasing x. Having these results in mind one can understand the observed EPR spectrum as due in a wider sense to magnetically isolated Cu(1) polyhedra. If neighbored sites (1) or (2) are occupied by Cu^{2+} exchange coupling will immediately induce EPR

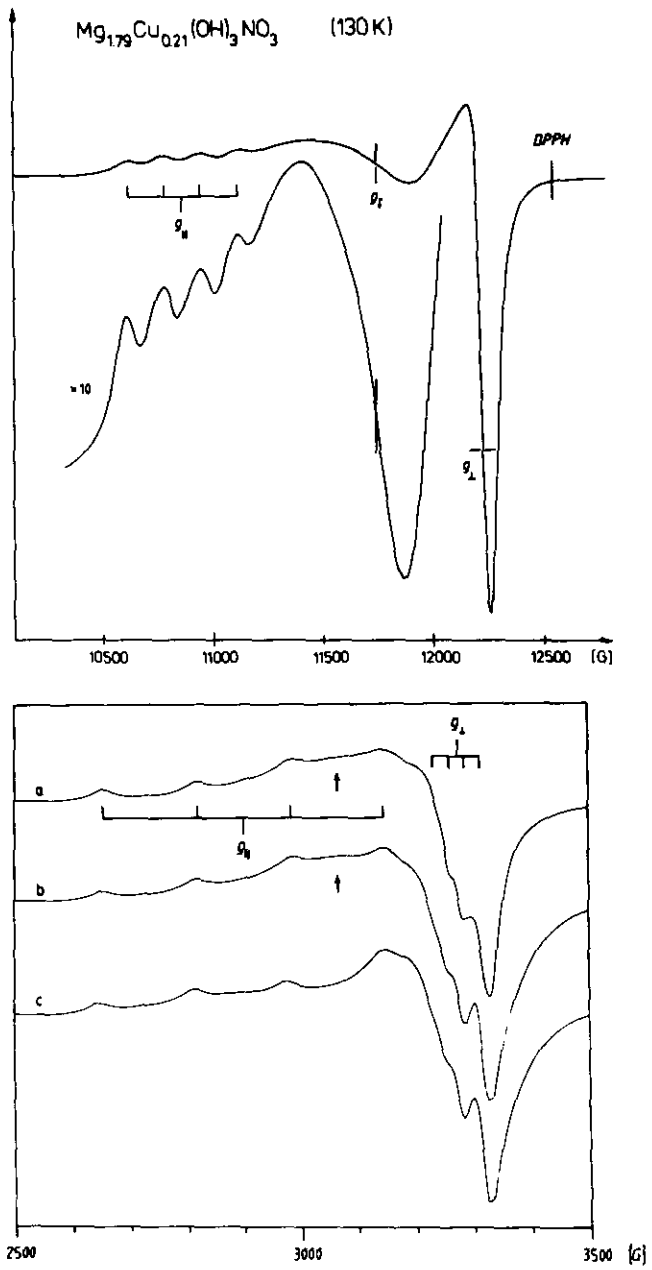

FIG. 5. EPR spectrum of $Mg_{1.79}Cu_{0.21}(OH)_3NO_3$ at Q (top) and X-band frequencies (bottom, (a)) and at 130 and 105 K, respectively. The Q-band spectrum contains an isotropic spectral component (presumably due to exchange coupling). The simulated X-band spectrum (c) corresponds to a superposition of spectra with and without hyperfine coupling in an intensity ratio 1 : 1, while in spectrum (b) an additional isotropic spectral component is taken into account (intensity ratio 3 : 3 : 1). The simulation parameters are explicitely mentioned in the text and Table 1.

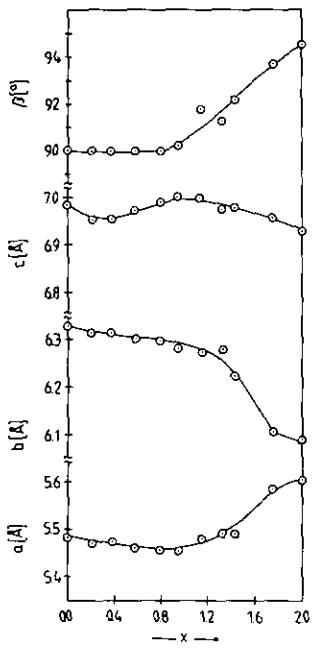

FIG. 6. Unit cell parameters of $Mg_{2-x}Cu_x(OH)_3NO_3$ mixed crystals in dependence on x.

silence for the pairs. This explains why the intensity of the EPR signals is drastically reduced with increasing x.

The simulation of the X-band spectrum is only possible if spectral components with hyperfine splitting (Lorentzian line shape, $\Delta H_{1/2} = 15$ G) and without it (Gaussian line shape, $\Delta H_{1/2}(\|) = 180$ G, $\Delta H_{1/2}(\perp) = 60$ G) in a 1 : 1 intensity ratio are superimposed (Fig. 5 bottom, curve c). Such behavior is expected, because exchange coupling between isolated Cu^{2+} centers first wipes out the hyperfine splitting. Increasing coupling strength leads to an averaging of the g-tensor components, and indeed a simulation with the additional inclusion of an isotropic signal at $g_i = 2.14$ (Gaussian line shape, $\Delta H_{1/2} = 100$ G, 15% intensity contribution) improves the agreement with the experimental spectrum (Fig. 5 bottom, curve b). If the Cu^{2+} centers further approach each other with increasing x, the exchange integral is enhanced and finally induces EPR silence, as discussed already.

3. [CuO_6] *Polyhedron Distortions and Lattice Constants of* $Cu_xMe_{2-x}(OH)_3NO_3$ *Mixed Crystals* ($Me = Mg^{2+}$, Co^{2+})

The extent of the Jahn–Teller distortions of the [CuO_6] octahedra is reflected by the variations of the lattice constants of $Co_{2-x}Cu_x(OH)_3NO_3$ (2) and $Mg_{2-x}Cu_x(OH)_3NO_3$ with x (Fig. 6). In both cases the unit cell parameters behave similarly: a increases and b decreases with increasing Cu^{2+} concentration, while c remains practically unchanged. Geometric considerations show that the changes of a and b can be correlated with the local distortions of the CuO_6 polyhedra. The deviations from the regular octahedral geometry are described by the radial distortion parameter ρ, defined as

$$\rho = [2(dR_x^2 + dR_y^2 + dR_z^2)]^{1/2}, \qquad [5]$$

where dR_i ($i = x, y, z$) are the deviations of the corresponding metal–ligand distances from their mean (octahedral) values. The values ρ' for site 1 and ρ'' for site 2 in $Cu_2(OH)_3NO_3$ (Table 1) are $\approx$0.51 and $\approx$0.41 Å, respectively. Assuming in first approximation that the alterations δa and δb of the lattice constants a and b with decreasing x are essentially caused by variations of the axial spacings R_a, and that the atomic positional parameters do not change during the substitution, we obtain

$$\delta a \approx (\sqrt{2}/3)(\delta\rho' + 2\delta\rho'')$$
$$\delta b \approx (\sqrt{2}/\sqrt{3})\delta\rho'. \qquad [6]$$

According to our basic result the Me^{2+} ions occupy nearly exclusively site (2) for $1.0 < x < 2.0$, and it follows from Eq. [6] and Fig. 6 that $\delta\rho' > 0$ and $\delta\rho'' < 0$ with decreasing x. The analysis of the eigenvalues of the tensor of finite deformations (8) leads to the same conclusion. The latter result is expected, because polyhedron (2) should reduce its distortion on substitution by a non-Jahn–Teller ion. It is difficult, however, to rationalize $\delta\rho' > 0$. Possibly the reduction of the distortion of the $Me(2)O_6$ polyhedra induces an enhancement of the $Cu(1)O_6$ octahedra by packing effects in the lattice, but more probably the assumption of positional parameters independent on x is not correct.

4. *Vibronic Coupling and the Origin of the Cation Distribution in Mixed Cystals* $Cu_xMg_{2-x}(OH)_3NO_3$

It is the aim of this section to explain the cation distribution of Cu^{2+} between sites 1 and 2 in dependence on x in terms of a microscopic model looking at the various contributions to the ground state energy of Cu^{2+}. These are the local Jahn–Teller energy within the two types of Me_6 octahedra, the strain energy due to the presence of different ligands (OH^- and NO_3^-) and finally the elastic interaction energies between the distorted octahedra (cooperative Jahn–Teller coupling). The ^2E_g ground state of Cu^{2+} in octahedral coordination is geometrically unstable with respect to vibrations of the same symmetry (Fig. 2). The two components Q_θ and Q_ε distort the nuclear coordination to D_{4h} and D_{2h} symmetries, respectively. If one expresses Q_θ and Q_ε in polar coordinates, $Q_\theta = \rho \cos\varphi$, $Q_\varepsilon = \rho \sin\varphi$, the ground state energy is given by (7)

$$E = (1/2)K_\varepsilon\rho^2 + A_1\rho. \qquad [7]$$

The harmonic term $(\frac{1}{2})\ K_\varepsilon\rho^2$ opposes displacements along the ε_g path and the linear vibronic energy $A_1\rho$ tends to destroy the octahedral configuration. Second order vibronic terms are neglected; thus E does not depend on φ in first approximation.

The parent octahedra are not regular, however, and the presence of different ligands in the coordination spheres of site 1 (trans-$Me(OH)_4(NO_3)_2$) and site 2 ($Me(OH)_5(NO_3)$) has to be accounted for. One may argue that the lower symmetry in such coordination suppresses the vibronic coupling (22). However, it has been shown, both experimentally (23) and theoretically (6), that vibronic interaction in such cases is still operative. The latter can be described by the same term $A_1\rho$ in Eq. (7). A_1 will be different for site 1 and 2, due to the presence of two NO_3^- ligands in the former and only one NO_3^- ligand in the latter Cu^{2+} coordination sphere. For the sake of simplicity we neglect this difference. However, a strain energy S_θ is introduced to account for the ^2E_g splitting and ground state lowering even without Jahn–Teller coupling. It can be shown, using the angular overlap model (AOM), that for the trans-$Cu(OH)_4(NO_3)_2$ site the energy S'_θ is given by

$$S'_\theta = |e_\sigma^{OH} - e_\sigma^{NO_3}|, \qquad [8]$$

where e_σ^{OH} and $e_\sigma^{NO_3}$ represent σ-antibonding AOM energy parameters, which refer to octahedral $Cu(OH)_6$ and $Cu(ONO_2)_6$ polyhedra, respectively. Half of this quantity has to be used for the $Cu(OH)_5(NO_3)$ site $2[S'_\theta = 2S''_\theta \equiv S_\theta]$. Because the ligand field of the O ligator atom in NO_3^- is distinctly weaker than the one in OH^-, both sites offer a geometry to the entering Cu^{2+} ions, which corresponds to a "tetragonal elongation" of D_{4h} (C_{4v}) symmetry. The extent of this elongation is expected to be considerably enhanced by the Jahn–Teller effect, with a stronger influence on site 2 than on site 1. According to this consideration, the groundstate splitting for site 1 and site 2, respectively, is (6)

$$\begin{aligned} \Delta E(1) &= 2(|A_1|\rho' + |S_\theta|) \\ \Delta E(2) &= 2(|A_1|\rho'' + 1/2|S_\theta|), \end{aligned} \qquad [9]$$

yielding $A_1 \approx -8000\ cm^{-1}\ Å^{-1}$ and $S_\theta \approx -2400\ cm^{-1}$. Here the experimental radial distortion parameters $\rho' = 0.51$ Å, $\rho'' = 0.41$ Å for $Cu_2(OH)_3NO_3$ and the ground state splittings $\approx$13,000 cm^{-1}, $\approx$9000 cm^{-1} deduced from the optical spectra were used (Table 1). Apparently the ligand strain and the vibronic Jahn–Teller coupling ($A_1\rho$) contribute to about $\frac{1}{3}$ and $\frac{2}{3}$ to the ground state splitting of site 1, respectively, while the strain energy is only $\frac{1}{4}$ of the total splitting for site 2. In evaluating the ρ-parameters we have not taken into account that the octahedral

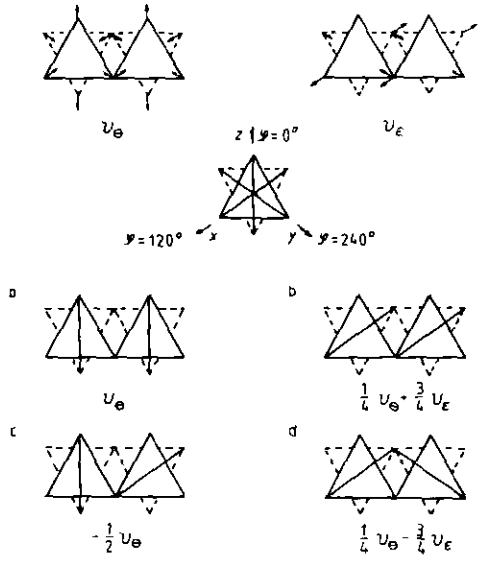

FIG. 7. Crama and Maaskant (25) parametrization of pair interactions between Jahn–Teller distorted octahedra in hexagonal layers of edge shared elongated CuO_6 octahedra: definition of v_θ, v_ε (top), and types of possible interactions (below). Estimated coupling energies for (a), (b), (c), and (d) are 2700, 975, −1350, and 375 cm^{-1}, respectively.

Cu–ONO_2 spacings are usually larger than the Cu–OH distances (24), because in our case the averaged Cu–O bond lengths in both sites are equal (2.11 Å), in spite of the presence of one and two ONO_2^- ligands, respectively (Fig. 1).

Let us now consider the interactions between neighboring Jahn–Teller centers, restricting to nearest neighbors only. Adopting a parametrization proposed by Crama and Maaskant for the coupling between chains of face-connected octahedra in hexagonal perovskites of the type $ACuX_3$ (25), which is symmetry equivalent to the present case of octahedra sharing common edges, we have the following dependence of the interaction energy of a pair of Jahn–Teller octahedra on their distortion coordinates ρ and φ:

$$V_{int} = \rho_i\rho_j(v_\theta \cos\varphi_i \cos\varphi_j + v_\varepsilon \sin\varphi_i \sin\varphi_j). \qquad [10]$$

ρ_i and ρ_j specify the extent of the local distortions of the two CuO_6 polyhedra, while φ_i and φ_j characterize their "directions." Since we deal with octrahedra, which are tetragonally elongated along the z, x, or y axis, the angular parameters have the values $\varphi_{i(j)} = 0°$, 120°, and 240°, respectively (Fig. 2), assuming D_{4h} symmetries in a crude approximation. v_θ and v_ε parameterize the pair potentials for octahedra distorted corresponding to $\varphi_i = \varphi_j = 0°$ and 90°, respectively (Fig. 7). Subdividing the lattice of $Me_{2-x}Cu_x(OH)_3NO_3$ mixed crystals into two sublattices (1) and (2),

$$[Cu_yMe_{1-y}]^{(1)}[Cu_{x-y}Me_{1-x+y}]^{(2)}(OH)_3NO_3,$$

with mean local distortions ρ' and ρ'' for the sites 1 and 2 occupied by Cu^{2+} and Mg^{2+} (Co^{2+}), we can follow the changes in the configurational energy in dependence on the distribution of Cu^{2+} between the two sublattices. The local Jahn–Teller and strain energies (Eqs. [11a, b]) as well as the contributions due to the cooperative elastic interactions between the octahedra (Eqs. [11c–e]) per formula unit are ($T = 0$ K)

$$y[(1/2)K_\varepsilon\rho'^2 + S_\theta + A_1\rho'] \quad [11a]$$

$$(x-y)[(1/2)K_\varepsilon\rho''^2 + S_\theta/2 + A_1\rho''] \quad [11b]$$

$$2(1/4)y^2\rho'(1)\rho'(1')(v_\theta - 3v_\varepsilon) \quad [11c]$$

$$2(x-y)^2\rho''(2)\rho''(2')v_\theta \quad [11d]$$

$$2[-(1/4)\rho'\rho''y(x-y)(v_\theta + 3v_\varepsilon)]. \quad [11e]$$

Expression [11c] considers the electronic coupling within sublattice 1, with two interactions of type d in Fig. 7 and $\rho'(1)$ being the variable distortion of the considered $Me(1)$ polyhedron under the influence of the two neighbored polyhedra (1'). Similarly, Eq. [11d] accounts for the two interactions of a $Me(2)$ polyhedron of type a in Fig. 7. Finally, as can be also deduced from Fig. 1, a Me(1) polyhedron is coupled to four neighboring $Me(2)$ polyhedra, which constitute two pairs of the interaction types c and d in Fig. 7, with interaction energy as given in Eq. [11e]. Minimizing the total energy per formula unit with respect to ρ' and ρ'' one obtains

$$\begin{aligned} y(K_\varepsilon\rho' + A_1) + 1/2y^2\rho'(v_\theta - 3v_\varepsilon) \\ - 1/2y(x-y)\rho''(v_\theta + 3v_\varepsilon) = 0 \\ x-y)(K_\varepsilon\rho'' + A_1) + 2(x-y)^2\rho''v_\theta \\ - 1/2y(x-y)\rho'(v_\theta + 3v_\varepsilon) = 0 \end{aligned} \quad [12]$$

The coupled equations can be solved for $Cu_2(OH)_3NO_3$ ($x = 2$, $y = 1$) with respect to the interaction parameters v_θ and v_ε, using the experimental ρ' and ρ'' values, the deduced A_1 parameter, and a reasonable value for the force constant of the ε_g mode ($K_\varepsilon \approx 16{,}500$ cm^{-1} Å^{-2} (26). The resulting magnitudes for v_θ and v_ε are ≈2700 and ≈400 cm^{-1}, respectively.

If one calculates the total configurational energy (Eq. [11]) for the compound $CuMg(OH)_3NO_3$ ($x = 1$) for the two distributions $y = 1$ (Cu^{2+} on site 1) and $y = 0$ (Cu^{2+} on site 2), with the estimated values for A_1, K_ε, S_θ, v_θ, v_ε, one obtains a configurational energy in the former case which is lower by about 2000 cm^{-1}, in agreement with the experiment. This value is somewhat larger than the difference of the contributions due to the ligand strain for sites 1 and 2 (Eqs. [11a, b]: $1/2|S_\theta| \approx 1200$ cm^{-1}). Apparently the comparatively more pronounced distortion of site 1 is the decisive energetic factor.

It is surprising at first sight, that a cooperative ordering of the Cu^{2+} polyhedra is observed in $Cu_2(OH)_3NO_3$, which involves pair interactions with predominantly positive energies (see Fig. 1 and pair interactions (a(2x)), d(2x), and c in Fig. 7). One would rather have expected an "antiferrodistortive" ordering pattern (14) according to c in Fig. 7, which might be realized in $Cu(OH)_2$. Unfortunately this compound crystallizes in a rather different structure type (27) so that a direct comparison is not possible. The presumable reason that the energetically most favorable "antiferrodistortive" pair interaction (c in Fig. 7) is not chosen seems to be the presence of two different kinds of ligands, which is not accounted for explicitely in Eqs. [11c–e]. Every oxygen ligator atom is bonded to three Cu^{2+} ions. While the three O(1)–Cu bonds are long (Fig. 1), the corresponding $O_h(21,22)$–Cu spacings are short; from the three $O_h(1)$–Cu bonds finally two are short and one is long. Because the bond strength of the oxygen atoms O(1) in the NO_3^- group versus Cu^{2+} is rather weak compared to the one of OH^-, a kind of cooperative order is realized, which certainly would not be observed in an isostructural compound with equal ligands, as in $Cu(OH)_2$ for example. Here it is expected that every ligator atom is bonded to three Cu^{2+} ions via one long and two short bonds. The role of the bridging ligands in determining the cooperative-elastic ordering in compounds with Jahn–Teller unstable cations is discussed more rigorously elsewhere (26). The *electronic* energy contributions due to cooperative Jahn–Teller forces, which are also not taken into account in our simple model and which are frequently very large in structures with strongly interconnected polyhedra, can be substantiated by a concept, which considers the bonding capacity of an interconnecting ligand as constant within narrow limits.

SUMMARY

The spectroscopic, structural and magnetic investigation of mixed crystals $Me_{2-x}Cu_x(OH)_3NO_3$ [Me: Co^{2+}, Mg^{2+}] yielded the following results:

1. In the concentration region $0 < x \lesssim 1$ the $Me(OH)_4(ONO_2)_2$ site (1) is substituted with great preference by Cu^{2+}, because it provides a larger Jahn–Teller distortion than site (2) with a pseudooctahedral $Me(OH)_5(ONO_2)$ coordination.

2. The magnetic exchange interactions between the Cu^{2+} ions in the unit cell are rather large and of antiferromagnetic nature. EPR spectra can be detected up to $x \approx 1.5$ and are due to magnetically isolated Cu^{2+} ions in site (1).

3. The observed cooperative Jahn–Teller order of elongated octahedra in $Cu_2(OH)_3NO_3$ is not the one expected

on the basis of a minimization of the elastic interactions. The comparatively weaker bonding strength of the oxygen ligator atom in NO_3^- leads to an order pattern, in which this atom is bonded to three Cu^{2+} ions in equally large distances, while the OH ligands are nearly exclusively involved in short bonds to the three surrounding Cu^{2+} ions.

ACKNOWLEDGMENTS

The support of the Bulgarian National Scientific Research Foundation, the Deutsche Forschungsgemeinschaft, and the Fonds der Chemischen Industrie is gratefully acknowledged. The authors owe thanks to Prof. Dr. J. Pebler (Marburg) for the magnetic measurements.

REFERENCES

1. K. Petrov and L. Markov, *Silikattechnik* **37,** 197 (1986).
2. N. Zotov and K. Petrov, *Z. Kristallogr.* **190,** 235 (1990).
3. N. Zotov, K. Petrov, and M. Dimitrova-Pankova, *J. Phys. Chem. Solids* **51,** 1199 (1990).
4. N. Zotov, K. Petrov, and S. Hristov, *Thermochim. Acta* **198,** 61 (1992).
5. H. Effenberger, *Z. Kristallogr.* **165,** 127 (1983).
6. D. Reinen and M. Atanasov, *Magn. Reson. Rev.* **15,** 167 (1991).
7. I. B. Bersuker, "The Jahn–Teller Effect and Vibronic Interactions in Modern Chemistry." Plenum, New York, 1984.
8. N. Zotov and K. Petrov, *J. Appl. Crystallogr.* **24,** 227 (1991).
9. L. Markov, K. Petrov, and R. Joncheva, *Russ. J. Inorg. Chem.* **30,** 3023 (1985).
10. J. Macicek, "PDI—A Computer Program for Powder Data Interpretation." IAM BAS Report, 1988.
11. G. Kortüm, "Reflexionsspektroskopie." Springer-Verlag, Berlin, 1969.
12. A. Ludi and W. Feitknecht, *Helv. Chim. Acta* **46,** 2226 (1963).
13. C. Friebel, *Z. Naturforsch. B* **29,** 295 (1974).
14. D. Reinen and C. Friebel, *Struct. Bonding* **37,** 1 (1979).
15. B. R. McGarvey, *J. Phys. Chem.* **71,** 51 (1967).
16. A. Abragam and M. H. L. Pryce, *Proc. R. Soc. London A* **230,** 169 (1955).
17. G. Steffen, D. Reinen, H. Stratemeier, M. J. Riley, M. A. Hitchman, H. E. Matthiew, K. Recker, F. Wallrafen, and J. R. Niklas, *Inorg. Chem.* **29,** 2123 (1990).
18. D. Reinen and J. Wegwerth. *Physica C* **183,** 261 (1991).
19. D. Reinen, Theoret. *Chim. Acta Berlin* **5,** 312 (1966).
20. M. Atanasov, S. Angelov and I. Mayer, *J. Mol. Struct. (Thermochem)* **187,** 23 (1989).
21. D. J. Hodgson, *Progr. Inorg. Chem.* **19,** 173 (1975).
22. (*a*) J. K. Burdett, *Inorg. Chem.* **14,** 931 (1975); (*b*) J. K. Burdett, *Inorg. Chem.* **20,** 1959 (1981).
23. M. J. Riley, M. A. Hitchman, D. Reinen, and G. Steffen, *Inorg. Chem.* **27,** 1924 (1988).
24. W. Stählin and H. R. Oswald, *Acta Crystallogr. Sect B* **26,** 860 (1970).
25. W. J. Crama and W. J. A. Maaskant, *Physica B* **121,** 219 (1983).
26. M. Atanasov, U. Kesper, B. L. Ramakrishna and D. Reinen, *J. Solid State Chem.* **105,** 1 (1993).
27. (*a*) H. Taggi, H. R. Oswald, *Acta Crystallogr.* **14,** 1041 (1961); (*b*) H. R. Oswald, A. Reller, H. W. Schmalle and E. Dubler, *Acta Crystallogr. Sect. C* **46,** 2279 (1990).